ISSN: 2319-5967
ISO 9001:2008 Certified
International Journal of Engineering Science and Innovative Technology (IJESIT)
Volume 3, Issue 4, July 2014

Efficient multibeam sonar calibration and performance evaluation

Yannick Perrot[a)], Patrice Brehmer, Gildas Roudaut, Peter Gerstoft, and Erwan Josse
Yannick Perrot, Patrice Brehmer, Gildas Roudaut, and Erwan Josse
IRD (Institut de Recherche pour le Developpement), LEMAR (Marine Research Laboratory), BP. 70, F-29280 Plouzané, FRANCE
Peter Gerstoft
Scripps Institution of Oceanography, University of California San Diego, La Jolla, CA 92093-0238, USA

Abstract: ***Quantitative applications of mobile multibeam sonar in aquatic ecology and fisheries require accurate and efficient in-tank calibration methodologies. Calibration factors for a Simrad SM20 multibeam sonar are experimentally extracted thereby enabling sonar estimation of target strength and volume backscattering strength. Measured and modeled sonar characteristics are systematically compared and show good overall correlation. Due to the limited angular span of the sonar head array, well quantified sonar operation is restricted to an equatorial angular sector of only 80° (vs. rated 120°) in 'imaging' mode. In 'echo-sounder' mode, the 'high' power transmit setting appears to introduce artifacts. A routine in-tank measurement procedure is described which for given multibeam sonar minimizes the time required for quality multibeam calibration.***

Keywords: **Sonar, Multibeam, Calibration, SM20, In-tank, Fisheries acoustics, Procedure.**

I. INTRODUCTION

From the pioneering works of Cochrane *et al.* [1] and Foote *et al.* [2] on the calibration of scientific multibeam sonar (MBS), such devices have been used in numerous studies to monitor aquatic organisms [3]. Stocks of small pelagic fish are often assessed using the echo integration technique. The calibration procedure ensures good time series quality and accurate measurements [4], [5]. As MBS is used to investigate various topics in marine ecology [6]–[10] and fisheries [11]–[13], it is important to calibrate them, check their performance and carry out quantitative applications by extracting calibrated target strength (TS, in dB) and volume-backscattering strength (S_v , in dB) from MBS data [14]–[16].

The multibeam sonar calibration protocol, developed by Foote [2], describes in detail the device plan, the measurements and methods to realize them, the measurement uncertainties and possible errors, and calibration results for the SM20 MBS. Cochrane [1] supply in detail all the sonar theory needed for multibeam sonar calibration. Based on the MBS theory of [1], the MBS calibration protocol developed by [2] was implemented to calibrate a 200-kHz Simrad SM20 MBS in a seawater tank and to evaluate its performances. The measured calibration factors (equivalent two-way beam angles and system gains) and the measured performances of the sonar transmission (two-dimensional transmit directivities) and reception (two-dimensional beam patterns and elemental directivity of the sonar head array) are investigated and compared with theoretical performances. Besides the performances estimated in [2] for the 200-kHz SM20 MBS echo-sounding (ES) mode that uses an external transducer for transmission, this study also estimates the sonar performances in imaging (IM) mode that uses the SM20 sonar head array in transmission. For both operating modes, SM20 performances (e.g. elemental directivities, sonar head array transmission, transmit levels for the different power setting), not presented in [2], are discussed in this work.

A lot of multibeam sonars are not, or rarely, calibrated because it's a difficult and a time consuming operation to execute. It is then important to perform routine in-tank calibration for MBS efficiently, since their calibration is time consuming and that MBS for quantitative applications deployed from various platforms (*e.g.* vessels, buoys, remotely operated vehicle, bottom stations) requires in-tank calibration. An in-tank measurement procedure is proposed to optimize the calibration time duration by evaluating, according to the characteristics of the sonar to be calibrated, the most efficient way (measurement strategy, beam sampling optimization) to realize all the measurements describes in [2] by respecting all the methodologies and requirements of the Foote's calibration protocol. This procedure allows efficient beam sampling and accurate planning of the calibration time according to the beam sampling; the latter defines the calibration precision. The procedure consist of 1) a

ISSN: 2319-5967
ISO 9001:2008 Certified
International Journal of Engineering Science and Innovative Technology (IJESIT)
Volume 3, Issue 4, July 2014

measurement strategy, *i.e.* how to scan the beams in the equatorial and polar planes of the sonar, 2) the sampling of the beams in the equatorial and polar planes, 3) the scanning speeds used in both planes, 4) the sonar to calibration sphere distance and 5) the MBS characteristics, *i.e.* number of beams, equatorial and polar beam resolutions.

The beam sampling is a compromise between duration and required quality (defined by the user application). When a MBS is initially calibrated, the procedure finds the optimal beam sampling based on the MBS characteristics. Based on the initial calibration, a routine measurement procedure for the next calibrations of this MBS can be implemented. The SM20 performance evaluation presented here validated the efficiency of the MBS in-tank measurement procedure. These results also supply a performance evaluation applicable to any 200-kHz SM20 MBS.

II. MATERIAL AND METHODS

A. The Simrad SM20 multibeam sonar system

The Simrad SM20 MBS operates at 200 kHz with two separate operating modes, referred to as imaging (IM) and echo-sounding (ES). This MBS operates at three transmission power levels, low, medium and high power corresponding to 50, 100 and 150 % nominal transmit power. For both operating modes, no envelope weighting is applied to the transmit pulse [17]. The IM mode use the SM20 sonar head transducer array in transmission and echo reception to form, over a total angular sector of 120°, 128 receive beams with 1.5° theoretical beam widths in the equatorial plane (along the transducer array, item 8 in Fig. 1) and 17° in the polar plane (normal to the transducer array, item 7 in Fig. 1). This array consists of 80 rectangular elements (2.54 x19.05 mm) positioned, with an equal inter-element spacing of 1.116°, on a circular arc with 20 cm radius. The IM mode nominal source level is 203 dB (re. 1µPa @ 1m). For the ES mode, the sonar head array is used just for reception, and transmission is performed by a 50 element vertical array of length 27.6 cm (item 5 in Fig. 1) located in the central polar plane of the sonar head array. The angular spans of the transmit beam are estimated as 150° in the equatorial plane and 1.6° in the polar plane. By forming a Mills cross [18, pp. 60], 128 resulting beams, with beam widths of 1.5° in the equatorial plane and 1.6° in the polar plane, are formed over a 120° angular sector. The ES mode nominal source level is 210 dB (re. 1µPa @ 1m). The near field distance is 10.5 m [5, pp. 151]. Thus only ranges in the far field, *i.e.* beyond 10.5 m, are used.

B. Instrumented seawater testing tank facility

The calibration experiment was carried out in the Ifremer (Plouzané, France) seawater deep tank (see http://www.ifremer.fr/metri/pages_metri/infrastructure/brest_basin.htm). The tank is 50 m long and 12 m wide, with a depth of 20 m for the first 12.5 m of its length, and then 10 m. The measured seawater temperature (16.6°C) and salinity (35.5 psu) were homogeneous throughout the water column, giving an absorption coefficient of $\alpha = 0.07025$ dB/m calculated from [5, Eq. (2.20)] and sound speed of 1514 m/s (wavelength 1514/200 = 7.6 mm).

The MBS and its rotator system were mounted midway between both tank sides on a movable platform positioned 6.25 m from the back of the tank (Fig. 1). The equatorial plane of the MBS receiving beam fan (plane running through the sonar head array elements, item 7 in Fig 1) is in the horizontal plane and the polar plane (item 8 in Fig 1) of the sonar head array is vertical. The center of the sonar head array was positioned at 4.36 m depth. The MBS could rotate in the equatorial plane using a step-by-step 360° arc rotator (Compumotor AX drive model), which enabled small increments with an accuracy of 0.03°. A programmable controller piloted the rotation automatically according to the configuration (beginning and end angular positions, and angular speed) scheduled previously by the operator. The rotator PC and the MBS acquisition PC were synchronized. During the data processing stage, the date, the time and the angular position of each rotation increment were recorded from a customized algorithm to associate each rotator increment with a recorded ping. The BK8105-3 omnidirectional hydrophone, calibrated by Brüel&Kjaer, measured the one-way directivity of the MBS transmission in the equatorial and polar planes. The receiving sensitivity and source level calibration of this hydrophone projector is traceable to NIST (National Institute of Standards and Technology); at 200 kHz, it had a calibrated source level of 136.98 dB (re. 1 µPa @ 1 m) and a receiving free-field voltage sensitivity of -218.53 dB (re. 1 V/µPa).

The calibration target was a 38.1 mm diameter tungsten-carbide calibration sphere with nominal target strength 'TS' of 38.9 dB at 200 kHz (given by the manufacturer), density of 14 900 kg m^{-3} and longitudinal and

ISSN: 2319-5967
ISO 9001:2008 Certified
International Journal of Engineering Science and Innovative Technology (IJESIT)
Volume 3, Issue 4, July 2014

transverse sound speeds of 6853 m/s and 4171 m/s, similar TS can be computed [5, pp. 71-75]. The reflection from this target was used to measure the two-way beam patterns of the MBS in the equatorial and polar planes. From a second movable platform, the hydrophone or alternatively the calibration target, suspended by a single line of monofilament nylon, were positioned on the central beam axis of the MBS at 10.60 m from the transducer face. A manual system, including a block and a ruler, was used to measure the depths of the hydrophone or the target.

Strong echoes from the tank sides were present in the beam side lobes from 6.25 m range, corresponding to the distance between the sonar and the tank sides. The high echo level of this reverberation generated a noisy zone on the multibeam image from 6.25 m range despite the side lobes were 22 dB lower than the main lobe. This effect is also observed when MBS is tested at sea with the equatorial plane of its receiving beam fan vertically. In this configuration, the seabed echo is present in the beam side lobes by producing this noisy zone beyond the distance between the sonar and the seabed. Nevertheless, to calibrate in the far field of the sonar emission, the calibration sphere was positioned (10.6 m range) in this noisy zone, knowing that the signal-to-noise ratio (SNR) measured on the sphere echo was sufficient (SNR ~ 20 dB for IM mode and ~ 24 dB for ES mode) for performing calibrations. For the direct paths, the first echo reverberation from the two tank sides occurred from 2*6.25 = 12.5 m, *i.e.* beyond our observation range. The reverberation effects from the free surface or the bottom of the tank was not important, since for the widest polar plane beam width of 17° gives the first beam echo reverberation from the free surface at 4.36/tan(17°/2) = 29 m range. The received signal was range-gated to eliminate this free-surface and bottom reflections.

To apply this method to other MBS, the measurement errors must be carefully determined or evaluated for the tank used for testing and MBS characteristics (Section II-A for SM20 MBS). As described above for the SM20 calibration, the sources of uncertainty [19, pp. 17-21] are sound speed, sonar positioning [20], rotator angular accuracy, echoes from the tank sides, surface and bottom, the precision of the predicted TS of the calibration sphere for the MBS operating frequency [21]–[22], hydrophone performances. If the MBS characteristics (especially, its far field range and beam widths in both planes) are adapted to the sizes of tanks used to avoid multiple echoes, the proposed measurement procedure (Section II-E) can be implemented to calibrate the MBS.

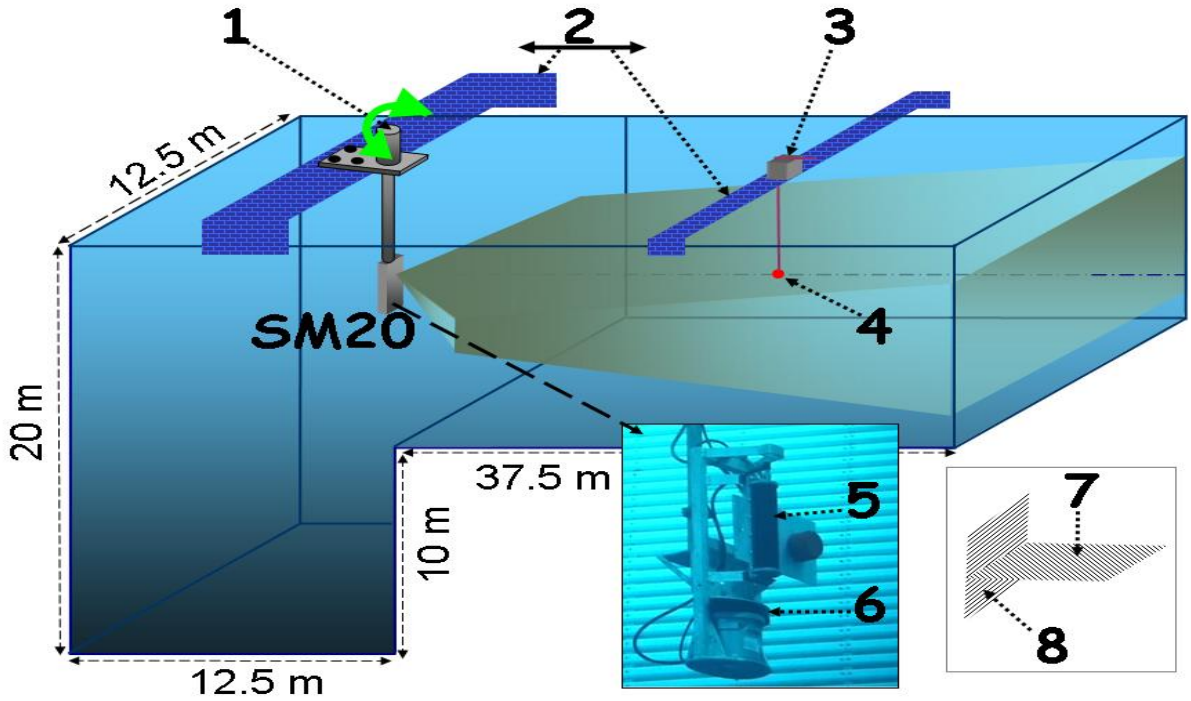

FIG. 1. (Color Online) Diagram of the instrumented seawater tank configured for multibeam sonar (MBS) calibration. 1) Automatic rotator (360° arc, 0.03° accuracy, PC control). 2) Moveable platforms. 3) Manual system with a ruler gauge for the vertical displacement of the sphere. 4) Tungsten-carbide calibration sphere or hydrophone. 5) MBS external transducer. 6) MBS sonar head. 7) MBS equatorial plane. 8) MBS polar plane.

ISSN: 2319-5967
ISO 9001:2008 Certified
International Journal of Engineering Science and Innovative Technology (IJESIT)
Volume 3, Issue 4, July 2014

C. Calibration theory

MBS calibration enables estimating sonar calibration parameters for each beam and extracting calibrated TS and S_v from MBS data. These measured calibration parameters were introduced to describe the deviations of a real sonar from its ideal performances.

For a MBS synthesizing a receive beam at the azimuth θ_b (Fig. 2), TS and S_v are determined according to formulae in [1]:

$$TS(\theta_b,t) = 20\ \log(v_{BF}(\theta_b,t)) + C_{cal}(\theta_b), \quad (1)$$

$$S_v(\theta_b,t) = TS(\theta_b,t) - 10\ \log\left(\Psi_D(\theta_b)\, R^2(t)\, \frac{c.\tau_{nom}}{2}\right), \quad (2)$$

where $v_{BF}(\theta_b,t)$ is time-dependent resultant beam formed voltage at angle θ_b pre-corrected to a TVG response of $40\log(R(t)) + 2\,\alpha\, R(t)$, *R(t)* time-dependent sonar target range, *c* sound speed (m/s), τ_{nom} nominal sonar-pulse duration. For each angle θ_b, the system gain (or calibration factor) for the beam $C_{cal}(\theta_b)$ and the equivalent two-way beam angle $\Psi_D(\theta_b)$ (or beam width factor) were measured. The system gain is experimentally given by:

$$C_{cal}(\theta_b) = TS_{cal} - 20\ \log\left(v_{BF}(\theta_b,t_{cal})\right), \quad (3)$$

Where TS_{cal} is the TS of the calibration sphere, and $v_{BF}(\theta_b,t_{cal})$ is the resultant beam formed voltage for the sphere echo. The equivalent two-way beam angle $\Psi_D(\theta_b)$ is estimated from the measured two-way equatorial beam pattern using the approximation in [1, Eq. (25)]:

$$\Psi_D(\theta_b) \cong \frac{\sqrt{17.4}}{k\ w} \int \left(D_{S\theta}(\theta_b,\theta)\, D_{R\theta}(\theta_b,\theta)\right)^2 d\theta, \quad (4)$$

where $\{(D_{S\theta}(\theta_b,\theta)\, D_{R\theta}(\theta_b,\theta))\}$ is proportional to the beam formed amplitude for a target at angle θ_b, *k* the acoustic wave number, and *w* the length (in meter) of the array in the latitudinal (normal to fan) direction. $D_{S\theta}$ and $D_{R\theta}$ are transmit and receive directivity functions. When envelope weighting is applied to the transmit pulse, *e.g.* SIMRAD ME70 MBS [4], an additional calibration correction factor must be estimated to compensate for this. As the SM20 pulse is not weighted, this was not needed here. For both modes, SM20 MBS theoretical characteristics (two-dimensional beam patterns, elemental directivities, transmit directivities) were calculated by a Matlab code. The theoretical transmit equatorial directivity function and the theoretical receive beam formed equatorial directivity functions were computed in [1, Eqs. (26) and (29)]. Then, for each operating mode, the theoretical beam patterns of Fig. 5 were obtained from the product of these theoretical transmit and receive equatorial directivity functions. The theoretical sonar system gain curves C_{cal} (Fig. 6a and 6b) correspond to the peak level of each theoretical beam patterns without the amplitude normalization. The theoretical equivalent two-ways beam angles (Fig. 6c and 6d) were computed from the Eq. (4) using the $D_{S\theta}$ and $D_{R\theta}$ theoretical functions. For a comparison between estimated and measured MBS performances, it is essential to perform these theoretical calculations with the same array weighting function and the summation normalization as used by the MBS beam former. For the SM20, the beam forming uses Hamming weighting in [1, Eq. (36)] (without the factor 2 in the denominator) and the summation normalization uses in [1, Eq. (9)]. The theoretical elemental directivity of the SM20 sonar head array was extracted from in [1, Table I]. However, in this work, we used the measured elemental directivities to compute the theoretical beam patterns.

TABLE I. Estimated and measured source levels (dB re. 1 µPa @ 1m) for the three SM20 power settings: high (150 % of nominal power), medium (100 % nominal power) and low power (50 % of nominal power). Sonar mode: 'IM' Imaging and 'ES' Echo sounder

Source level (SL in dB)	IM mode		ES mode	
	Estimated	Measured	Estimated	Measured
High power	206.5	205.0	213.5	214.0
Medium power	203.0	203.0	210.0	210.0
Low power	197.0	191.0	204.0	199.0

ISSN: 2319-5967
ISO 9001:2008 Certified
International Journal of Engineering Science and Innovative Technology (IJESIT)
Volume 3, Issue 4, July 2014

D. Data validation

The significance level *p* of the correlation coefficients *r* ([23]–[24]), used in the measured data validation procedure described below, is calculated using a Student t-test with the degree of freedom (dof) corresponding to the measurements points for each parameter. The test assumes that each of the populations being compared is Gaussian with the same variance. These assumptions were tested using a Kolmogorov–Smirnov test for the normality and a F-test for the variance equality. From these tests, a correlation is significant when the hypothesis of absence of correlation can be rejected by assuming a 5 % error risk.

The methodology to validate the measured data consists of comparing the individual measured and estimated beam patterns by calculating their correlation coefficient and testing its significance using the t-test (as above). If a non-significant correlation is obtained and the sources causing the lack of correlation are not identified, the measured beam pattern is rejected. Then, the beam pattern measurements are not relevant for calibration parameter extraction or the beam angular sampling is not sufficient. Otherwise, the beam pattern is considered in compliance with the theory and deemed as relevant for calibration parameters extraction. When all the beam patterns were tested, both MBS calibration parameters are extracted from beam patterns. The measured calibration parameters are validated by calculating the correlation coefficient between measured and estimated values and testing its significance using a t-test. A significant correlation means that the measured beam patterns for all beam angles θ_b are coherent between them, in terms of measured levels for C_{cal} [Eq. (3)] and spatial distribution for Ψ_D [Eq. (4)]. Otherwise, the measurements are not in compliance and the measurement error source must be identified or the beam angular sampling is not sufficient for sonar calibration. The measurement uncertainties have to be considered in the analysis of MBS performance. When the agreement between prediction and measurement is poor, they can be included to refine the analysis and evaluate their impacts.

E. In-tank measurement procedure

As the beam sampling in the equatorial and polar planes defines the quality and the duration of the calibration, a routine measurement procedure requires optimizing both parameters. Thus, when a MBS is initially calibrated, the beam sampling in both planes is over-sampled. Afterwards optimal sampling parameters are obtained; *e.g.* [2] showed that a beam sampling of 0.1° in both planes assures a good calibration quality in tank and might thus represent beam over-sampling.

Beam samplings in both planes are optimized using an iterative process: 1) Beam patterns with a high beam sampling (over-sampling) and corresponding calibration parameters are validated by applying the data validation procedure described in Sect. II-D. 2) Beam samplings are reduced in steps (the decimation factors are integer to avoid interpolated values in the decimated data). 3) Decimated beam patterns are tested by applying the data validation procedure. 4) Steps 2 and 3 are continued to find the lowest beam samplings that provides significant correlation. Note that the under sampling of the beam response does not create aliasing, as that is related to under sampling in phone space.

To measure the MBS two-way equatorial beam patterns, the calibration sphere is positioned on the central beam axis at the maximum of sensitivity (see Fig. 1). To bring the target in front of the first beam, the MBS is rotated $\theta_{fan}/2$ clockwise (θ_{fan} is the total equatorial angular span of the beam fan), see Fig. 2. Then, the MBS data recording starts with automatic rotating the MBS θ_{fan} counterclockwise in steps of $\Delta\theta_{eq}$ (the beam angular sampling in the equatorial plane). The MBS ping rate and the time between sonar rotations (ΔT_r) are chosen to acquire at least two pings for each angular position. These rotations enable scanning, at the centre of the polar plane, the equatorial plane. All the equatorial beam patterns are calculated from the target echo return at each angular position. To estimate the MBS two-way polar beam patterns (Fig. 2), the rotation of θ_{fan} counterclockwise is repeated for N_{po} vertical positions of the calibration sphere on either sides of the polar plane central axis, with one on the axis. With θ_{po}, the theoretical polar beam width, the calibration sphere is then vertically displaced in angular steps of $\Delta\theta_{po} = \theta_{po}/(N_{po} - 1)$ which define the beam angular sampling

ISSN: 2319-5967
ISO 9001:2008 Certified
International Journal of Engineering Science and Innovative Technology (IJESIT)
Volume 3, Issue 4, July 2014

in the polar plane. To scan the beam widths and side lobes, it is recommended adding angular margins on θ_{fan} and θ_{po}.

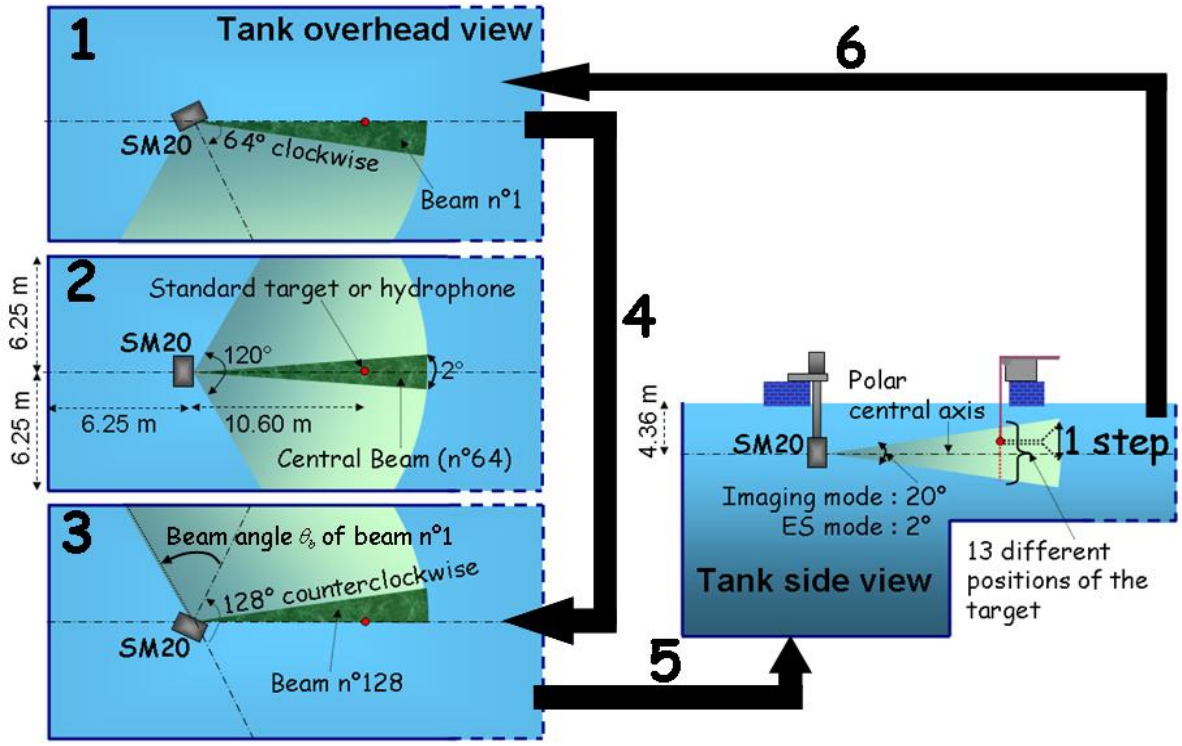

FIG. 2. (Color Online) Schematic of the multibeam sonar (MBS) calibration procedure in the seawater tank.1) Initial 2) central and 3) last angular position of the MBS equatorial beam scanning. 4) 128° counterclockwise rotation of the MBS in 0.2° steps to scan the equatorial plane of every beam. 5) Vertical displacement of the target by one step around the polar central axis before scanning again every beam in the equatorial plane. 6) Beam scanning in the equatorial plane (stages 1-4) is repeated for 13 vertical target positions in order to scan the polar plane.

The duration (τ_{cal} in s) to scan the beam fan in both planes using the procedure is:

$$\tau_{cal} = \left(\frac{\theta_{fan}}{\Delta\theta_{eq}} + 1\right) \Delta T_r \; N_{po} = \left(\frac{\theta_{fan}}{\Delta\theta_{eq}} + 1\right)\left(\frac{\theta_{po}}{\Delta\theta_{po}} + 1\right) \Delta T_r , \qquad (5)$$

This procedure was implemented to measure the two-way beam patterns of the SM20 MBS. The sonar target range was then 10.6 m, the ping rate was 2 pings/s, ΔT_r = 1 s and, including their respective added angular margins, $\theta_{fan} = 128°$, $\theta_{po} = 21.4°$ for IM mode and $\theta_{po} = 2.6°$ for ES mode. Thus, the over-sampled beams were fixed to $\Delta\theta_{eq} = 0.2°$ for both SM20 operating modes and $\Delta\theta_{po} = 1.78°$ for IM mode and $0.22°$ for ES mode. The calibration would then last $\tau_{cal} = 02$ h 19 min, Eq. (5). To find the optimal beam sampling, the measured beam patterns in ES mode were decimated by considering half of the measurement points in each beam ($\Delta\theta_{eq} = 0.4°$ and $\Delta\theta_{po} = 0.44°$) and compared with their theoretical values. With these decimated samplings, the calibration would only last $\tau_{cal} = 38$ min. During the SM20 calibration experiment, the transmitted signal generated a pulse lasting 300 μs (≡ 60 λ) in IM mode and 200 μs (≡ 40 λ) in ES mode. For both modes, the transmit-power was in high power setting, and the TVG (Time Varied Gain) was $40\log(R) + 2\alpha R$, where R is the observation range (m) and α the acoustic absorption coefficient (dB/m). For both SM20 modes, equatorial beam patterns are presented in Fig. 5 with the TS values calculated by using the system gain and the beam formed voltages $v_{BF}(\theta_b, t)$ in dB measured at the target range, Eq. (1).

ISSN: 2319-5967
ISO 9001:2008 Certified
International Journal of Engineering Science and Innovative Technology (IJESIT)
Volume 3, Issue 4, July 2014

Beam patterns are then plotted on an absolute TS scale, with a peak level corresponding to the TS of the calibration sphere. To estimate the SM20 performances in terms of beam side lobes levels and positions, the measured beam patterns were also synthesized without applying Hamming weighting in beam forming. This raises the side lobe levels above the noise floor.

To measure MBS one-way transmit directivity function in the equatorial and polar planes; the calibration sphere is replaced by the hydrophone. Then the same measurement procedure as previously described to measure the beam patterns from the standard calibration sphere is carried out. The hydrophone is then used in reception, and the MBS in transmission. For these measurements, the SM20 transmitted in high power setting, pulses lasting 240 µs, for both modes. To evaluate the stability of the MBS transmission relative to the pulse duration, the source levels are measured at the hydrophone for a set of different pulse durations. In the case of the SM20, seven different pulse durations were considered (75, 100, 150, 200, 250, 300, and 500 µs).

The elemental directivities of a MBS array are measured in both planes using the hydrophone in transmission and the MBS array only in reception. Using the hydrophone instead of the calibration sphere, the same measurement procedure (as above) used to measure the two-way beam patterns was implemented using, at each rotation increment, the hydrophone pulse received by each element of the MBS array (*i.e.* using the raw data directly before beam forming).

The sphere echo stability is also evaluated with a chosen pulse repetition by measuring, from the central beam, the sphere echo over a sufficient time period. For the SM20 calibration, this was performed over a 40 s time period, with a 4 pings/s pulse repetition, for both modes, 3 transmit power levels, and 5 pulse durations (75, 100, 200, 300, and 500 µs).

It is important to evaluate the calibration sphere positioning at the maximum of sensitivity in the central beam, the calibration sphere vertical displacement (used to scan the MBS polar beam widths), and the calibration sphere movement stability before starting the procedure. After each calibration sphere displacement, it is important to wait for its stabilization (~5 min).

III. RESULTS

The measured equatorial directivity of the central element (element n°40) of the SM20 head data is shown in Fig. 3, with the manufacturer estimated single element directivity [1]. Although the measured and estimated elemental directivities were significantly correlated ($r = 0.90$, $p < 0.05$, $dof = 620$) (Fig. 3), the measured and estimated equatorial –3 dB beam widths were different with values of 31° and 65.4°, respectively. Subsequently, all the theoretical characteristics of the SM20 were computed by using the measured elemental directivities. The SM20 transmit directivities for both modes measured by the hydrophone in the equatorial and polar planes are shown in Fig. 4. The estimated (from the manufacturer) and measured maximum source level under high, medium and low power settings for both modes are presented in Table I. A significant difference in low power setting was noted (up to 6 dB for IM mode and 5 dB for ES mode) between estimated and measured source levels. In high power setting, this difference was lower (1.5 dB for IM mode and 0.5 dB for ES mode) and no difference was found in medium power setting, corresponding to the nominal power of the MBS.

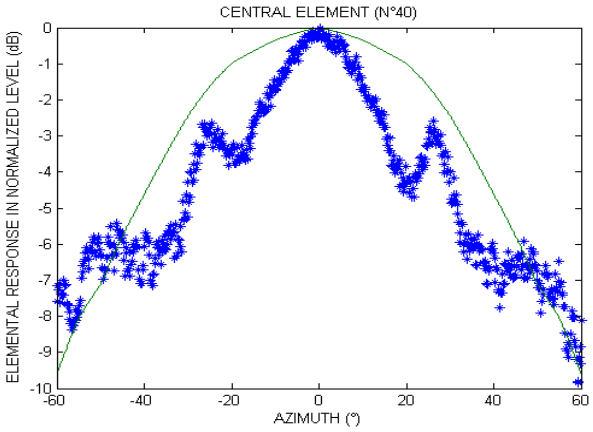

FIG. 3. Measured (*) and estimated (solid) equatorial-plane directivities of the central element (n° 40) of the multibeam SM20 sonar head array

ISSN: 2319-5967
ISO 9001:2008 Certified
International Journal of Engineering Science and Innovative Technology (IJESIT)
Volume 3, Issue 4, July 2014

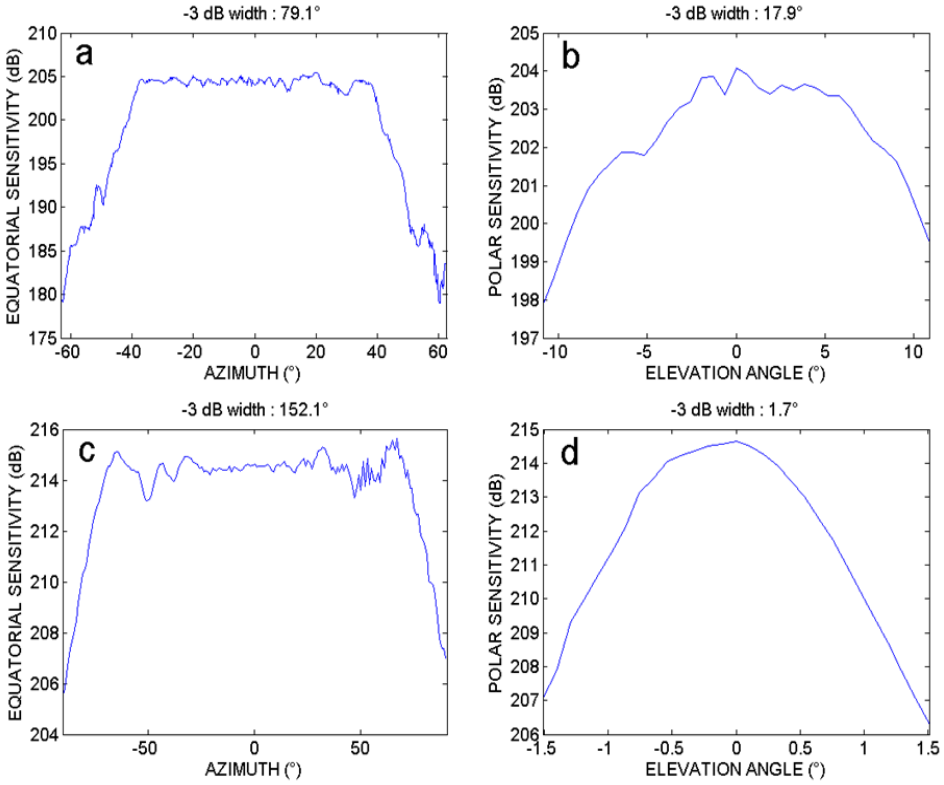

FIG. 4. SM20 transmit directivities measured using the hydrophone in (a) equatorial and (b) polar planes for IM imaging mode, and in (c) equatorial and (d) polar planes for ES echo sounder mode.

TABLE I. Estimated and measured source levels (dB re. 1 µPa @ 1m) for the three SM20 power settings: high (150 % of nominal power), medium (100 % nominal power) and low power (50 % of nominal power). Sonar mode: 'IM' Imaging and 'ES' Echo sounder.

Source level (SL in dB)	IM mode		ES mode	
	Estimated	Measured	Estimated	Measured
High power	206.5	205.0	213.5	214.0
Medium power	203.0	203.0	210.0	210.0
Low power	197.0	191.0	204.0	199.0

Otherwise, the source levels remained stable for all 7 pulse-durations for both modes and the three transmit power levels. The maximum variations were always lower than 0.5 dB. The measured angular span (-3 dB) of the transmit directivity were 79.1° and 17.9° for the IM mode and 152.1° and 1.7° for the ES mode in the equatorial and polar planes, respectively.

The two-way equatorial beam patterns for IM mode (Fig. 5a) and ES mode (Fig. 5b), measured from the calibration sphere enabled estimation of the equivalent two-way beam angle, Eq. (4), whereas the resultant beam formed voltage for the sphere echo measured by each beam was used to estimate the system gain, Eq. (3). The estimated and the measured values of these two calibration factors are shown in Fig. 6 for both modes. A set of equatorial beam patterns is presented in Fig. 5. The beam widths of the central beam in the equatorial and polar planes were respectively 1.9° and 16.7° for IM mode and 1.4° and 1.5° for ES mode. For ES mode, an increase was observed in the measured equatorial beam width (up to 3°) depending on the rise of the beam angles around the central beam to ± 60°, and a mean level of the first side lobes 14 dB below the maximum (without Hamming weighting). The correlation between the estimated and measured curves for the two calibration factors corresponding to the ES mode (Fig. 6b and 6d) was significant ($r = 0.99$ with $p < 0.05$, dof = 127 for system gain, and $r = 0.90$ with $p < 0.05$, dof = 127 for equivalent two-way beam angle).

ISSN: 2319-5967
ISO 9001:2008 Certified
International Journal of Engineering Science and Innovative Technology (IJESIT)
Volume 3, Issue 4, July 2014

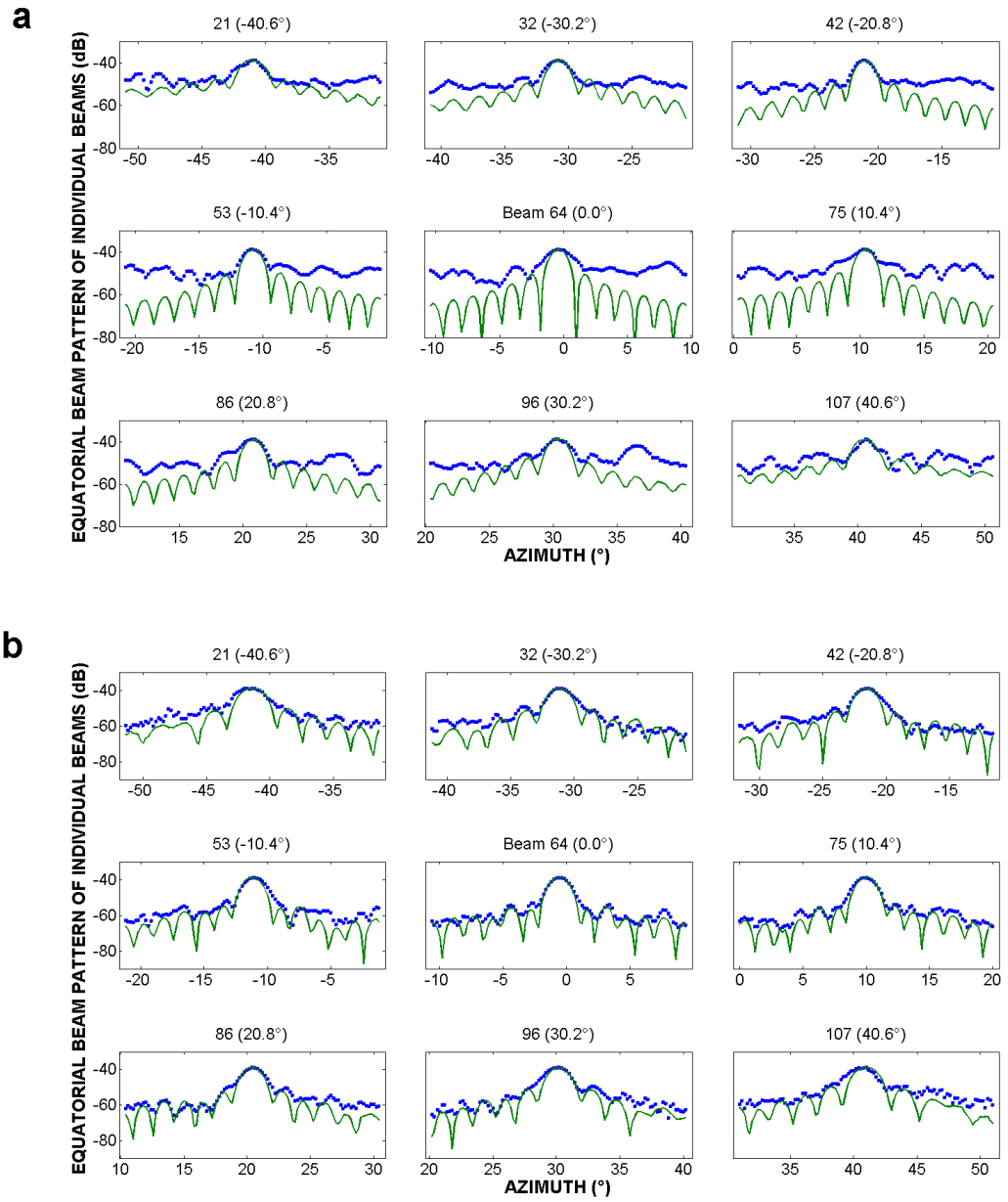

FIG. 5. (a) Equatorial-plane two-way beam patterns, from the calibration sphere (*) and estimated (solid), of a set of individual beams in IM imaging mode. (b) Equatorial-plane two-way beam patterns, measured from the calibration sphere (*) and estimated (solid), of a set of individual beams of the SM20 multibeam sonar in ES Echo sounder mode. Text in each subplot indicates the beam number and its beam angle.

For the beam angles below ±40° in IM mode, as for the ES mode, an increase was also observed in the measured equatorial beam width and a significant correlation ($r = 0.74$ with $p < 0.05$, dof = 90 for the system gain and $r = 0.67$ with $p < 0.05$, dof = 90 for the equivalent two-way beam angle) between the measured and estimated calibration factor curves (Fig. 6a and 6c). However, for the beam angles beyond ±40° in IM mode, the measured equatorial beam widths were randomly distributed and their corresponding measured and estimated equivalent two-way beam angles were also uncorrelated. For IM mode, even without Hamming weighting, the SNR was too weak to estimate the side lobes positions and levels. The measured equatorial beam width (with Hamming weighting) ranged from 2.1–4.5° for ES mode (depending on beam angle), and the mean level of the measured first side lobes was -22 dB.

ISSN: 2319-5967
ISO 9001:2008 Certified
International Journal of Engineering Science and Innovative Technology (IJESIT)
Volume 3, Issue 4, July 2014

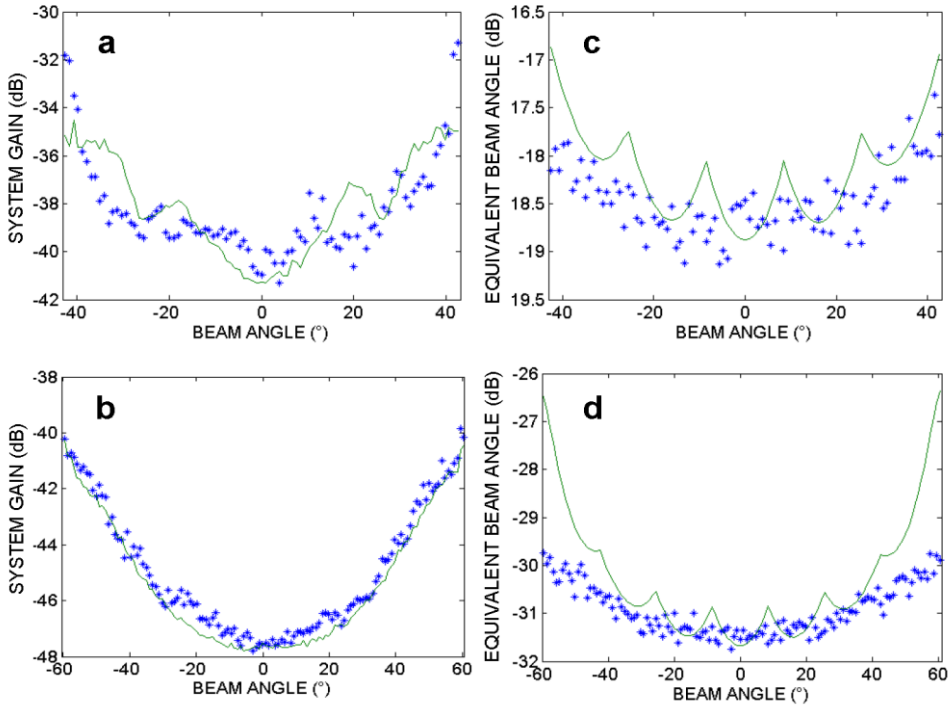

FIG. 6. Measured (*) and estimated (solid) system gains (a) and equivalent two-way beam angles (c) for beam angles below ± 40° in IM imaging mode. (b-d) the same for all the beams in ES echo sounder mode.

For each two-way equatorial beam pattern, the correlation between the measured and estimated curves was significant for all the beam angles in ES mode (mean correlation among all beams is r = 0.80 with $p < 0.05$, dof = 100) and for the beam angles below ±40° in IM mode (mean correlation among these beams is r = 0.71 with $p < 0.05$, dof = 100). For both modes the polar beam patterns were similar for all beams with polar beam widths in accordance with the hydrophone estimations. For both modes, the correlation between estimated and measured two-way polar beam patterns was calculated only for the central beam (r = 0.68 with $p < 0.05$, dof = 12 for IM mode and r = 0.77 with $p < 0.05$, dof = 12 for ES mode).

When the measured two-way beam patterns in ES mode were calculated using only half of the measurement points in each beam ($\Delta\theta_{eq} = 0.4°$ and $N_{po} = 7$), the correlation between the measured and estimated equatorial beam patterns remained significant for all the beam angles in ES mode (the mean correlation among all the beams is then r = 0.79 with $p < 0.05$, dof = 50). The estimated and measured polar beam patterns of the central beam in ES mode also remained significantly correlated (r = 0.71 with $p < 0.05$, dof = 6). The measured beam widths of the central beam in the equatorial and polar planes were also similar to the case when all measurement points were used (when the values were not exactly the same, a maximum beam width difference of 0.03° was noted). The correlation between the estimated and measured curves for the two calibration factors for ES mode remained also significant (r = 0.97 with $p < 0.05$, dof = 63 for system gain, and r = 0.85 with $p < 0.05$, dof = 63 for equivalent two-way beam angle) when using just half of the measurement points.

The peak-to-peak (p-p) maximum amplitude variations of the sphere echo measured over 40 s were always less than 1 dB for IM mode in all transmit power levels and pulse durations. For ES mode in high power, this variation was between 1.3 dB (500-µs pulse) and 2.7 dB (75-µs pulse). For the medium and low powers, the variations were always less than 1 dB.

IV. DISCUSSION

The marked difference between the estimated and measured equatorial angular spans of the elemental directivity (Fig. 3) was due to the side lobes (at ±30°) on the measured directivity, which reduced the equatorial angular span of the main lobe (52.6 % reduction). These side lobes seems to be a physical characteristic of the sonar head array configuration. These side lobes do not seem due to a problem with the hydrophone transmission, as

ISSN: 2319-5967
ISO 9001:2008 Certified
International Journal of Engineering Science and Innovative Technology (IJESIT)
Volume 3, Issue 4, July 2014

the system gain (Fig. 6a) measured from the calibration sphere in IM mode (*i.e.* the sonar head array also in transmission) clearly reveal two side lobes, which result from those observed on the elemental directivity of the sonar head array. These side lobes might be a physical characteristic of the sonar head element mounting or inter-element interactions. To test this explanation, this measurement should be performed with another hydrophone and SM20 MBS. A conclusive test would be to measure the directivity of a single array element separated from the others. The reduced equatorial angular span of the elemental directivity increases the mean noise level in the MBS image. For a given sample of the MBS image, the beam forming consists of focusing each array element signal on this sample by introducing an appropriate time delay for each element and by summing all their resultant contributions. Thus, when the angular span of the elemental directivity is reduced, the number of elements that cannot observe a focus point well is increased, and this increases the noise level in the MBS image. However, as the correlation level (0.9) between the estimated and measured equatorial elemental directivities remains high, this increase of the noise level compared with the expected theoretical performances of this MBS is likely weak.

In ES mode, the equatorial and polar angular spans of the measured SM20 transmit directivity (Fig. 4) were all found to match theoretical predictions and the manufacturer's specifications. In IM mode, the report was the same for the transmit directivity, of which the 79.1° equatorial-plane angular span corresponds to the physical curvature angle of the sonar head array. Nevertheless, in terms of echo level continuity, this angular span measured by the hydrophone, was unexpectedly found to be insufficient to form a consistent sonar image at 120°. Indeed, in IM mode, it was systematically observed during the calibration an abrupt fall of the SNR from the calibration sphere for beam angles beyond ± 40°. At these azimuths, this resulted in a sudden disappearance of the sphere echo from the sonar image. Therefore, when the transmission signal was provided by the MBS in IM mode, the beams beyond ± 40° could not be calibrated. Thus, for quantitative applications of the SM20 in IM mode, it is necessary to use a reduced sector of 80° to obtain consistent echo levels for all beams.

For IM mode and for angles beyond ±40°, the two-way beam patterns, the 2D beam widths, and especially the side lobe levels and positions could not be measured accurately. This was due to the weak SNR from the calibration sphere caused by the small angular span of the transmit directivity. For these angles, equivalent two-way beam angles and system gains cannot be used to calculate TS and S_v. However, the measured two-way beam patterns (Fig. 5a and 5b) and calibration factors (Fig. 6), for angles below ±40° for IM mode and to the whole beam fan in ES mode, were well correlated with their theoretical estimates. However, even for the beams close to the central beam, the SNR from the calibration sphere remained too weak in IM mode to estimate the side lobes levels and positions. In contrast, in ES mode the SNR was sufficient to measure these side lobes for every beam, and their measured and estimated levels and positions consistently matched.

For both modes, the source levels measured in medium power level (100 % of nominal power) corresponded exactly to the estimated (Table I). This was not the case for low and high power (Table I) even though the sonar and the hydrophone were fixed between the measurements in the three power settings. Moreover, the same discrepancies were observed for all 7 pulse durations in both modes. During the stability evaluation of the signal received by the sonar head array, calibration sphere echo level measurements were also made for the three power settings. These sphere echo measurements showed differences between their echo levels in high and low power settings which were similar to the differences obtained from the hydrophone absolute measurements. Thus, the problem did not come from a measurement error or a hydrophone dysfunction, but resulted rather from the SM20 transmissions. Based on the measurements, the high power setting of the SM20 MBS corresponds to 158 % for ES mode and 126 % for IM mode of the nominal power (instead of 150 %) whereas the low power setting corresponds to 28 % for ES mode and 25 % for IM mode of the nominal power(instead of 50 %). To generalize this result, another SM20 system must be similarly calibrated.

The measured echo level of the calibration sphere over a 40 s period remained stable for all transmission power levels and pulse durations, except for ES mode in high power where the sphere echo level varied for all pulse durations. The sphere echo levels varied almost periodically, with maximum p-p amplitude (2.7 dB on a period of 2.5 s with 75 µs pulse duration). This phenomenon was discussed in [25] for a SIMRAD EK60 echo sounder (200 kHz). The effects were attributed to additional losses caused by non-linear acoustic propagation for a high-power, high-frequency, and high-directive source. However, this explanation cannot be verified from this MBS and it might only concern this SM20. To avoid this effect, the SM20 in ES mode should only be used in medium or low power.

ISSN: 2319-5967
ISO 9001:2008 Certified
International Journal of Engineering Science and Innovative Technology (IJESIT)
Volume 3, Issue 4, July 2014

Except for the unexpected echo levels in high and low power settings and the sphere echoes variation in high power for ES mode, this evaluation of the SM20 performances can be extended to other SM20 systems. The main recommendation is to consider only a sector of 80° (*vs.* rated 120°) around the central beam when the sonar is used in IM mode for quantitative applications. This avoids the problem of echo-level continuity due to the insufficient equatorial angular span of the sonar head array transmit directivity.

V. CONCLUSION

The good agreement between measured and estimated SM20 performances indicates the proposed measurement procedure works well. The high correlation between estimated and measured ES mode beam patterns using half of the measurement points showed that the number of beam samples can be reduced by a factor 2 in both planes while maintaining sufficient precision. The optimal beam sampling determined for SM20 system ($\Delta\theta_{eq} = 0.4°$ and $\Delta\theta_{po} = 0.44°$) will be used in the next routine calibration. The calibration would then theoretically last $\tau_{cal} = 38$ min instead of 02 h 19 min to scan the 128 beams of the SM20 in both planes. For routine in-tank calibration, a single polar beam pattern measurement of the central beam might be sufficient. In this case, the duration τ_{cal} of the calibration would be reduced by a factor N_{po} (here 13, see Eq. (5)).

This measurement procedure can be applied to any MBS if the tank sizes are sufficient for the calibration to be in the far field, avoiding reverberations from surface, bottom and tank sides overlapping the arrivals from the calibration sphere. The calibration sphere used must be adapted to the MBS operating frequency and bandwidth. Under these conditions, omnidirectional MBS can be routinely calibrated from the proposed measurement procedure using a 360° arc sonar rotator. If the MBS far field range exceeds the tank sizes, a calibration in near field can be performed [2, Section G] by using the theoretical near field beam forming [26] for the SM2000 system and this can also be adapted to other MBS systems.

It is planned to improve the tank calibration system further by adding a motorized programmable system to manage and control the vertical displacements of the calibration sphere and couple this to the MBS rotator PC control. Thus the calibrations of all the beams will be fully automated. To evaluate the calibration quality and the variability between the calibrations of two MBS, it will be useful to perform at sea a cross-calibration experiment simultaneously on the same target and in the same insonification plane for both MBS [27]. For routine MBS in-tank calibration, it might be useful to position the MBS with its equatorial beam fan in the vertical plane to have a configuration similar to the MBS calibration configuration at sea. It will then be necessary to have a deep tank (*i.e.* at least 15 m depth for far field measurements), an accurate automatic system for three-dimensional displacements of the calibration sphere to scan the beams in their two dimensions. With such a system, the MBS calibration could be done similarly as a classical in-tank scientific echo-sounder calibration.

ACKNOWLEDGEMENT

We thank Region Bretagne (CPER Bretagne) for contributing to funding of the MBS SM20. We thank the NSE-AS and STH-LTH teams of Ifremer (Plouzané, France), especially Naig Le Bouffant, Laurent Berger, Xavier Lurton and Carla Scalabrin for scientific suggestions as well as Anne Pacault and Xavier Bompais for assistance during the experiment.

REFERENCES

[1] N. A. Cochrane, Y. Li, and G. D. Melvin, "Quantification of a multibeam sonar for fisheries assessment applications," J. Acoust. Soc. Am., vol. 114, pp. 745-758, 2003.

[2] K. G. Foote, D. Chu, T. R. Hammar, K. C. Baldwin, L. A. Mayer, L. C. Jr. Hufnagle, and J. M. Jech, "Protocols for calibrating multibeam sonar," J. Acoust. Soc. Am., vol. 117, pp. 2013-2027, 2005.

[3] J. Simmonds and D. MacLennan, "observation and measurement of fish," in Fisheries Acoustics: Theory and Practice, 2nd ed. Oxford, UK, Ed. Blackwell, 2005, pp. 163-216.

[4] E. Ona, V. Mazauric, and L. N. Andersen, "Calibration methods for two scientific multibeam systems," ICES J. Mar. Sci., vol. 66, pp. 1326-1334, 2009.

[5] X. Lurton, An Introduction to Underwater Acoustics: Principles and Applications, 2nd ed. Berlin, GmbH & Co., 2010.

ISSN: 2319-5967
ISO 9001:2008 Certified
International Journal of Engineering Science and Innovative Technology (IJESIT)
Volume 3, Issue 4, July 2014

[6] F. M Gerlotto, P. A. Brehmer, P. G. Fernandes, D. G. Reid, P. Copland, S. Georgakarakos, and J. Paramo, "Application of multibeam sonar in marine ecology and fisheries research: New fields and limitations," J. Acoust. Soc. Am., vol. 114, pp. 2229-2229, 2003.

[7] K. J. Benoit-Bird, "Dynamic 3-dimensional structure of thin zooplankton layers is impacted by foraging fish," Mar. Ecol. Prog. Ser., vol. 39**,** pp. 61-76, 2009.

[8] A. S. Brierley and M. J. Cox, "Shapes of krill swarms and fish schools emerge as aggregation members avoid predators and access oxygen," Curr. Biol., vol. 20, pp. 1758-1762, 2010.

[9] P. Brehmer, J. Guillard, P. Caballero-Pinzon, and P. Bach, "Exploratory and Instantaneous Swimming Speeds of Amphidromous Fish School in Shallow-Water Coastal Lagoon Channels," Estuar. Coast., vol. 34, pp. 739-744, 2011.

[10] G. Di Maida, A. Tomasello, F. Luzzu, A. Scannavino, M. Pirrotta, C. Orestano, and S. Calvo, "Discriminating between Posidonia oceanica meadows and sand substratum using multibeam sonar," ICES J. Mar. Sci., vol. 68, pp. 12-19, 2011.

[11] O. A. Misund, A. Aglen, and E. Frønæs, "Mapping the shape, size, and density of fish schools by echo integration and a high-resolution sonar," ICES J. Mar. Sci., vol. 52, pp. 11-20, 1995.

[12] V. M. Trenkel, L. Berger, S. Bourguignon, M. Doray, R. Fablet, J. Massé, V. Mazauric, C. Poncelet, G. Quemener, C. Scalabrin, and H. Villalobos, "Overview of recent progress in fisheries acoustics made by Ifremer with examples from the Bay of Biscay," Aquat. Living Resour., vol. 22, pp. 433-445, 2009.

[13] J. Guillard, P. Balay, M. Colon, and P. Brehmer, "Survey boat effect on YOY fish schools in a pre-alpine lake: evidence from multibeam sonar and split-beam echosounder data," Ecol. Freshwat. Fish. vol. 19, pp. 373-380, 2010.

[14] K. G. Foote, H. P. Knudsen, G. Vestnes, D. N. MacLennan, and E. J. Simmonds, "Calibration of acoustic instruments for fish density estimation: a practical guide," ICES Coop. Res. Rep., vol. 144, 1987.

[15] D. Chu, K. C. Baldwin, K. G. Foote, Y. Li, L. A. Mayer, and G. D. Melvin, "Multibeam sonar calibration: Removal of static surface reverberation by coherent echo subtraction," in Proc. MTS/IEEE Oceans 2001, pp. 2498-2502, 2001.

[16] D. Chu, K. C. Baldwin, K. G. Foote, Y. Li, L. A. Mayer, and G. D. Melvin, "Multibeam sonar calibration: Target localization in azimuth," in Proc. MTS/IEEE Oceans 2001, pp. 2506-2510, 2001.

[17] C. Smith (Mesotech-Kongsberg-Simrad), private communication, September 2011.

[18] R. J. Urick, Principles of underwater sound, 3rd Ed. New York, McGraw-Hill, 1983.

[19] ANSI S1.20-2012, Procedures for Calibration of Underwater Electro acoustic Transducers. New York, American National Standards Institute, 2012.

[20] A. Islas-Cital, P. R. Atkins, K. Y. Foo, and R. Pico, "Phase calibration of sonar systems using standard targets and dual-frequency transmission pulses," J. Acoust. Soc. Am., vol. 130, pp. 1880-1887, 2011.

[21] K. G. Foote, "Optimizing copper spheres for precision calibration of hydro acoustic equipment," J. Acoust. Soc. Am., vol. 71, pp. 742-747, 1982.

[22] K. G. Foote, "Maintaining precision calibrations with optimal copper spheres," J. Acoust. Soc. Am., vol. 73, pp. 1054-1063, 1982.

[23] B. Scherrer, Bio statistique, Chicoutimi, Québec, G. Morin, 850 pp., 1984.

[24] MATLAB version 7.10.0. Natick, Massachusetts, The MathWorks Inc., 2010.

[25] F. E. Tichy, H. Solli, and H. Klaveness, "Non-linear effects in a 200-kHz sound beam and the consequences for target-strength measurement," ICES J. Mar. Sci., vol. 60**,** pp. 571-574, 2003.

[26] N. A. Cochrane, "Near-field considerations for Simrad-Mesotech SM 2000 multibeam sonar," Can. Tech. Rep. Fish. Aquat. Sci., Dartmouth, Can, Rep. 2417, 2002.

[27] Y. Perrot, J. Guillard, and E. Josse, "Convergence and divergence between two multibeam sonars (SIMRAD SM20 and RESON SeaBat 6012) used to extract the spatial, morphologic and energy parameters of fish schools," Fish. Res., vol. 106, pp. 378-385, 2010.